

Management strategy to mitigate voltage sags effects of a multi-motors system using ADALINE algorithm and cascade sliding mode control

Mounir Bensaid, Abdellfattah Ba-Razzouk, Mustapha El Haroussi

Systems Analysis and Information Processing (ASTI) Team, Mathematics, Computer, and Engineering Sciences Laboratory (MISI), Faculty of Science and Technology (FST), Hassan First University of Settat, Settat, Morocco

Article Info

Article history:

Received Jun 1, 2023

Revised Jul 4, 2023

Accepted Jul 29, 2023

Keywords:

ADALINE

Induction motor

IRFOC

Multi-motors system

Sliding mode control

Voltage sags

ABSTRACT

Multi-motor systems (MMS) find widespread use in various industrial applications, including plastic, paper, textiles, and steel rolling mills, where synchronized speeds are crucial for optimal operation. However, a significant limitation of these systems is their susceptibility to voltage sags, resulting in speed and synchronization loss, along with peak currents and torques during voltage recovery. This paper presents a comprehensive multi-motors management strategy aimed at attenuating the adverse effects of voltage sags. The proposed technique is based on principles that involve recovering the system's kinetic energy and leveraging the current reversibility of the converters. The control scheme comprises two main strategies: an adaptive linear neuron or later adaptive linear element (ADALINE)-based voltage sag detection algorithm utilizing least mean square (LMS) adaptation for rapid convergence using artificial neural networks, and a control scheme incorporating sliding mode speed controllers and indirect rotor field-oriented control (IRFOC). Additionally, a logic-based strategy for voltage sag attenuation completes the control framework. The effectiveness and efficiency of the proposed strategy are demonstrated through simulation results obtained using MATLAB/Simulink/SimPowerSystems.

This is an open access article under the [CC BY-SA](https://creativecommons.org/licenses/by-sa/4.0/) license.



Corresponding Author:

Mounir Bensaid

Systems Analysis and Information Processing (ASTI) Team

Mathematics, Computer, and Engineering Sciences Laboratory (MISI)

Faculty of Science and Technology (FST), Hassan First University of Settat

Settat, Morocco

Email: bensaidmounir.eae@gmail.com

1. INTRODUCTION

Many industrial applications require more than one motor. This is either because it is bulky in terms of volume (for example transport) or because the system necessitates distributed actuators (in the paper, textile and general web transport) [1], [2]. These applications become multi-motors systems (MMS) [3], and multi-converters systems [4]. Vehicle convoys (in the context of a smart highway with autonomous vehicles) and electric power transmission networks with generators and distributed loads are also included in this class of system [5]. MMS on the other hand are extremely sensitive to power supply disruptions [6]. Indeed, the most common disturbance problem is sudden voltage drops, also known as voltage sags [6]. The IEEE 1159 standard defines them as a 0.1 to 0.9 pu. decrease in root mean square (RMS) voltage over a time period ranging from 0.5 cycles to 1 minute [7]. Voltage-dips which are responsible for the majority of these

disturbances, are primarily caused by the start-up of large driving loads and power system faults such as lightning. Because these faults can never be eliminated in the electrical system, we must design equipment that can withstand the most common voltage dips [8], [9].

A single motor failure in a MMS, or a brief loss of synchronism between motors, can jeopardize the entire process and necessitate a complete shutdown. Furthermore, shutting down motor loads due to voltage dips has several consequences. For example, a loss of synchronism with the flux causes re-acceleration with high inrush currents, a low power factor, and a very long fault clearance time, causing the voltage dip to be prolonged. As a result, a reset procedure is required [10]. To reduce production losses and in some cases, limit the high currents required to restart motors after a voltage dip, equipment and strategies to keep the drives running during short and long voltage dips have been developed. The solutions are diverse, as are the costs: Changes to the protection logic to avoid premature shutdown, the use of backup power sources, changes to the power converter structure [10], [11], and use the rotating machines kinetic energy to maintain synchronism with the machine's flux to allow for efficient re-acceleration [12].

The main goal of this work is to develop a voltage sag management strategy for a MMS consisting of two AC drives with a common DC bus that are mechanically coupled by web with an adjustable tension. Furthermore, this work aims to contribute to the development of control methods that maintain the synchronism between the drives in the presence of voltage dips. The proposed management strategy is based on the principle of recovering the system's kinetic energy and the converter's current reversibility. This proposal makes no significant changes to the traditional structure of MMS with common DC bus and can be implemented using sliding mode controllers.

This paper is organized as follows: i) The nonlinear model of a simple winder system driven by two three-phase induction motors is presented in section 2; ii) The voltage-sag management strategy consists of three parts, presented in section 3. The adaptive linear neuron or later adaptive linear element (ADALINE) method, which generate the three-phase voltage-sag alarm signal quickly, the changes to M2 machine's operation mode based on logical conditions, and the modification of the control topology; iii) Simulation is carried out in section 4 to validate the relevance of the proposed solution; and iv) Finally, section 5 concludes the paper.

2. MATHEMATICAL MODELS OF THE WEB WINDING SYSTEM

A winding system, a good illustration of MMS, is composed of at least two rolls, mechanically coupled by a band of elastic material and driven by two motors. In a simple case, one motor winds the material at a given velocity while the other one serves to maintain a constant mechanical tension T_2 of the material as it is wound Figure 1 [3].

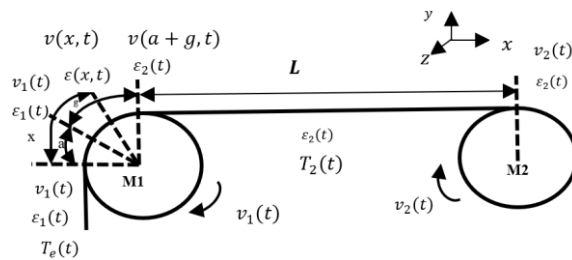


Figure 1. Web tension between two rolls

2.1. Mechanical models

Web-transport systems model is based on three laws, which enable to calculate the web tension between two rolls [13]:

- Hooke's law: To model the material's elasticity, the tension T is a function of its relative elongation ε and mechanical properties (Young's modulus and band section) $T = E \cdot S \cdot \varepsilon$.
- Coulomb's law: It expresses the variation in tension between the material and the roller in the contact zone.
- Mass conservation law: That shows the coupling between web velocity and web tension. These laws allow the calculation of web tension between two rolls.

The mechanical tension T_2 of the material between the rolls can be characterized as a function of the web length L and the linear speeds of the roller V_1 and V_2 . Where T_1 the input tension, E the Young modulus of the band and S the band section.

$$L \frac{dT_2}{dt} \cong ES(V_2 - V_1) + T_1 V_1 - T_2(2V_1 - V_2) \quad (1)$$

2.2. Electric drives models

Three-phase squirrel-cage induction machines are the most commonly used machines for converting electrical energy into mechanical energy. They can function both as motor and as generator. These machines are frequently used in high-power applications in the field of adjustable-speed drives.

A model based on the equivalent-circuit equations of the motor is generally sufficient to synthesize the control laws. Electrical dynamic model of three-phase Y-connected induction motor M_i can be expressed in the d-q synchronously rotating frame as (2) [5],

$$\begin{cases} \frac{d\omega_{mi}}{dt} = \mu_i \varphi_{r di} i_{sqi} - \frac{T_{ei}}{J_i} - \frac{f_i}{J_i} \omega_{mi} \\ \frac{d\varphi_{r di}}{dt} = -a_i R_{ri} \varphi_{r di} + a_i R_{ri} L_{mi} i_{s di} \\ \frac{di_{s di}}{dt} = \psi_{1i} + \frac{1}{\sigma_i L_{si}} u_{s di} \\ \frac{di_{sqi}}{dt} = \psi_{2i} + \frac{1}{\sigma_i L_{si}} u_{sqi} \\ \frac{d\theta_{si}}{dt} = p\omega_{mi} + a_i R_{ri} L_{mi} \frac{i_{sqi}}{\varphi_{r di}} \end{cases} \quad (2)$$

$$\text{with: } \psi_{1i} = -\eta_{1i} i_{s di} + p\omega_{mi} i_{sqi} + R_{ri} \left(-\eta_{2i} i_{s di} + a_i b_i \varphi_{r di} + a_i L_{mi} \frac{i_{sqi}^2}{\varphi_{r di}} \right),$$

$$\psi_{2i} = -\eta_{1i} i_{sqi} + b_i p\omega_{mi} \varphi_{r di} - p\omega_{mi} i_{s di} - R_{ri} \left(-\eta_{2i} i_{s di} + a_i L_{mi} \frac{i_{sqi} i_{s di}}{\varphi_{r di}} \right)$$

$$\mu_i = \frac{3pL_{mi}}{2J_i L_{ri}}; \eta_{1i} = \frac{R_{si}}{\sigma_i L_{ri}}; \eta_{2i} = \frac{L_{mi}^2}{\sigma_i L_{si} L_{ri}^2}; a_i = \frac{1}{L_{ri}}; b_i = \frac{L_{mi}}{\sigma_i L_{si} L_{ri}}$$

where $(u_{s di}, u_{sqi})$ are the stator voltages and $(i_{s di}, i_{sqi})$ are the stator currents in (d, q) coordinates. $\varphi_{r di}$ is the direct component of the rotor flux (the quadrature component of the rotor flux is equal to zero, i.e., $\varphi_{r qi} = 0$, due to indirect rotor field-oriented control (IRFOC). Thus, the electromagnetic torque is given by (3). Table 1 explains the parameters of the MMS.

$$T_{ei} = p \cdot \frac{M_{sri}}{L_{ri}} \cdot \varphi_{ri} \cdot i_{sqi} \quad (3)$$

Table 1. Rating parameters of the MMS

Symbol	Description	Value	Symbol	Description	Value
S	Enchainment section	2. 10 ⁻³ m ²	R_{si}	Stator resistance	0.7 Ω
L_b	Enchainment length	2 m	R_{ri}	Rotor resistance	0.31 Ω
E	Band Young modulus	0.2.10 ⁹ N/m ²	J_i	Inertia factor	0.0357 kg.m ²
C	DC link capacitor	1650 μF	f_i	Viscous friction factor	0.003 N.m.s
L	DC link inductance	115 μH	V_s	voltage	120/208 V
L_{si}	Stator inductance	80.6 mH	P	Nominal power	2 kW
L_{ri}	Rotor inductance	80.6 mH	N	Nominal speed	1750 rpm
L_{mi}	Mutual inductance	77.4 mH	p	Number of pole pairs	2

2.3. Behavior of the DC bus in voltage-sags mode

Bidirectional DC/AC converters are used to control three-phase machines, especially in MMS with a common DC bus. They offer the possibility to transfer power either, from the common DC bus to the machines or from the machines to the DC bus. Theoretically, Figure 2 shows a constant power flow between the machines is possible due to the reversibility of the converter [14].

During power interrupt or in rectifier blocked condition, the DC link voltage (V_{dc}) is directly affected by the operating mode of the machine. Consequently, when the machine operates in motor mode, V_{dc} decreases, and when the machine operates in generator mode, V_{dc} is increased. The rate of change, dV_{dc}/dt , is related to the capacity of the DC link, to the power of the machine, to the combined converter-machine efficiency and to the value of V_{dc} . $p_i = \omega_i T_{ei}$ is the electromagnetic power, with T_{ei} the electromagnetic

torque developed by the induction motor M_i , and $p_{dci} = P_{e_i}/\eta_i$ is the electric power of the inverter i , with η_i the inverter efficiency. Notice that $\eta_i \leq 1$ for motoring mode and $\eta_i \geq 1$ for generating mode.

Under the same condition, the dc-link voltage variation dV_{dc}/dt is a function of induction motors electromagnetic powers and the inverters efficiency. It will be enough to manage the power of the machines so that one of them can operate in motor mode when the other is working in generator mode, in order to maintain the electrical voltage of the DC-link constant. DC-link voltage regulation is possible in steady state if power relation (5) is satisfied.

$$\frac{dV_{dc}}{dt} = \frac{1}{CV_{dc}} \left(\frac{-T_{e1}\omega_1}{\eta_1} - \frac{T_{e2}\omega_2}{\eta_2} \right) \quad (4)$$

$$\frac{T_{e1}\omega_1}{\eta_1} = \frac{T_{e2}\omega_2}{\eta_2} \quad (5)$$

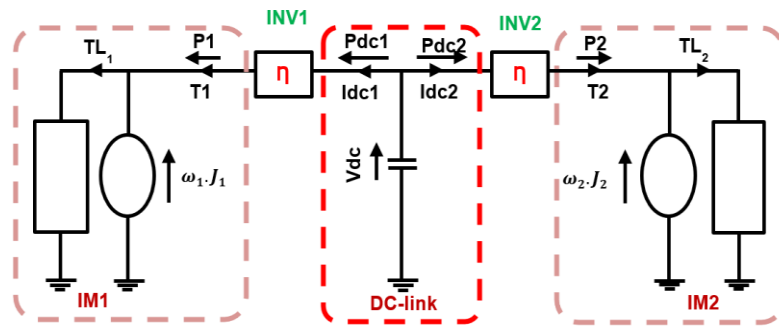


Figure 2. Equivalent circuit of two machines connected to a common DC bus

3. VOLTAGE-SAG MITIGATION SYSTEM

Figure 3 shows the structure of the management strategy to mitigate sags for MMS consisting of two levels of control:

- Control level 1: An ADALINE based voltage-sag detection algorithm with least mean square (LMS) adaptation and a logic strategy for voltage-sag mitigation including different operating modes definition.
- Control level 2: A control structure based on sliding mode speed controllers and IRFOC.

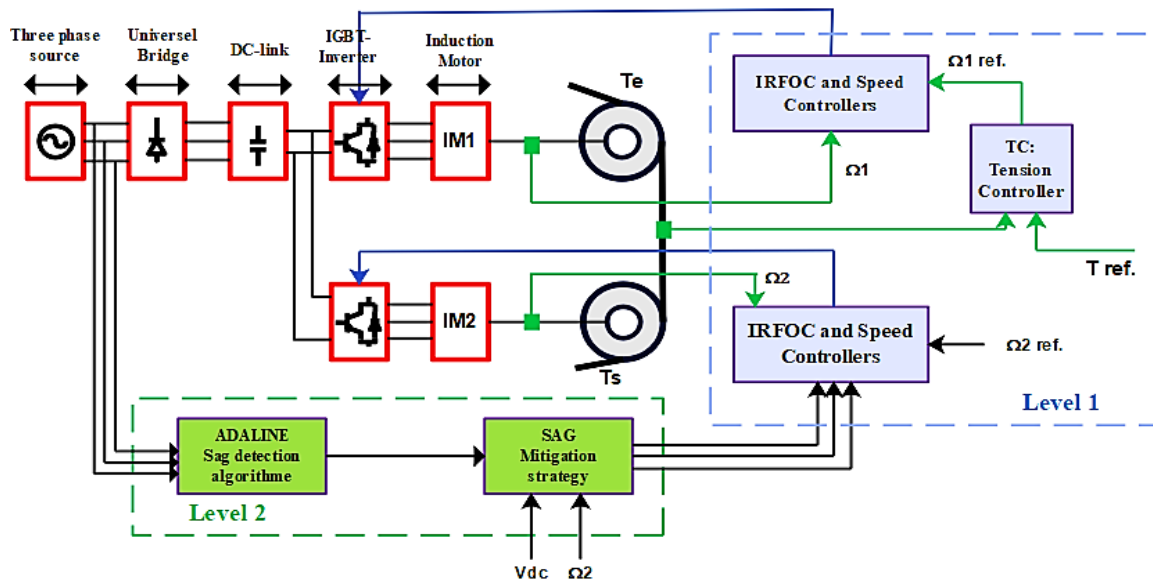


Figure 3. Sag mitigation strategy for two motors web coupled structure

3.1. Adaline method in rapid detection of voltage-dips

ADALINE belongs to the family of Perceptron's. It has a single neuron with a linear activation function and an input in the form of a vector $x(k)$. It was proposed and developed by Widrow [15]. The structure and algorithm of the ADALINE network is described in Figure 4 [7]. ADALINE has been successfully used to estimate the amplitude and phase of a signal's fundamentals.

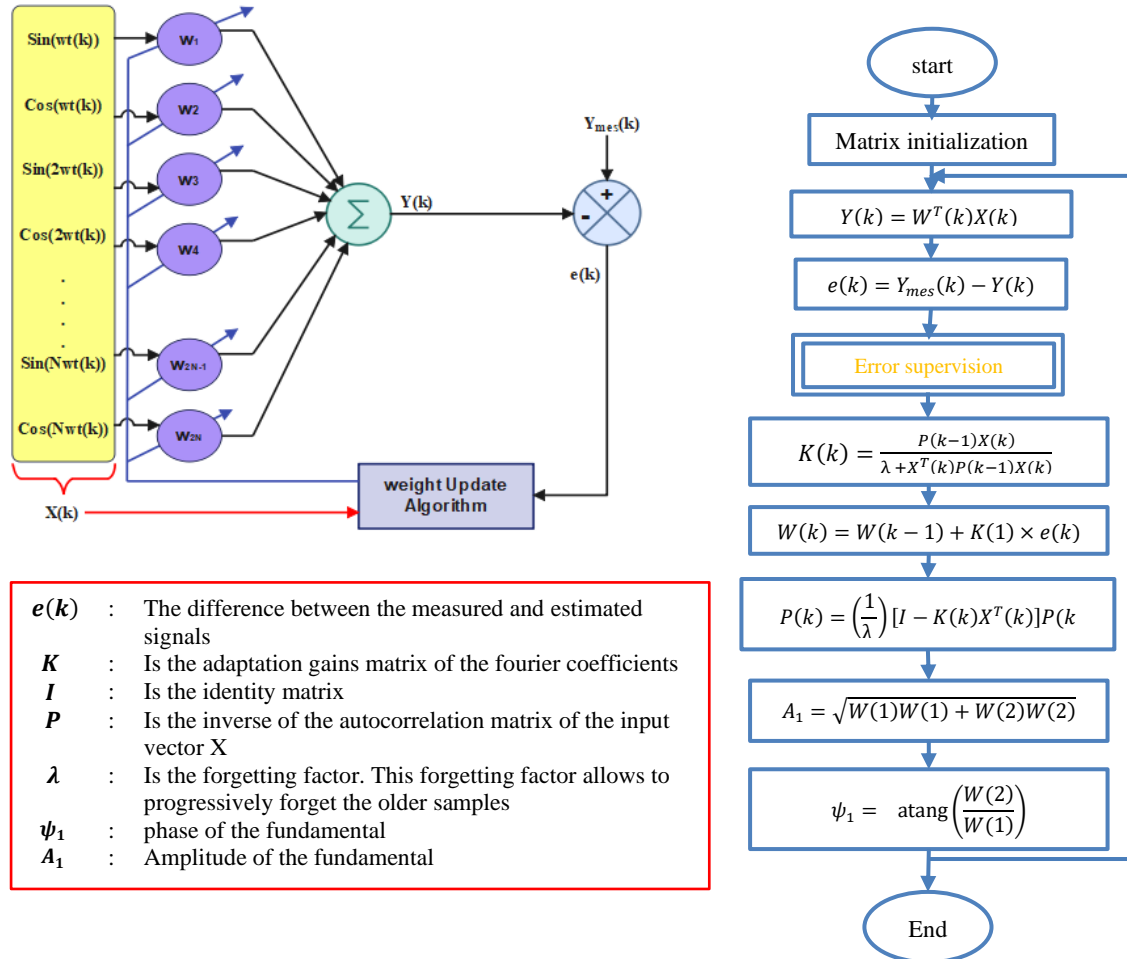


Figure 4. Structure and algorithm of the of ADALINE method (with error supervision)

3.2. Control structure

The control structure shown in Figure 3, is implemented using sliding mode control speed controllers, indirect rotor field-oriented controllers (IRFOC) and another sliding mode control controller is used for the web mechanical tension control with external web tension set point T_{ref} . This controller generates the speed set point for M1 in a cascade-control loop structure. A speed sliding mode controller (SSMC) is designed to control the speed of an induction motor fed by three phase voltage source inverters controlled by pulse width modulation (PWM) technique [16], [17].

In this work, the sliding mode control scheme is illustrated in Figure 5. Sliding mode controller is a nonlinear controller based on the principles of variable structure control. Similar to DC motors, speed control of induction motors can be realized in a cascaded control scheme [18], with a current controller in the inner loop and a speed controller in the outer loop. In general, the mechanical equation of an induction motor can be written as providing the reference currents i_{sdi}^{ref} and i_{sqi}^{ref} for the inner loop [19].

3.2.1. Rotor speed controller

Let ω_{mi}^{ref} be the motor rotor's desired mechanical angular speed. Design a switching function for speed control as: $S_{\omega i} = \omega_{mi}^{ref} - \omega_{mi}$, and the sliding surface's derivative is given as: $\dot{S}_{\omega i} = \dot{\omega}_{mi}^{ref} - \dot{\omega}_{mi}$ and

substituting the speed expression by the fifth (2), we have: $\dot{S}_{\omega i} = \dot{\omega}_{mi}^{ref} - \mu_i \varphi_{rdi} i_{sqi} + \frac{T_{ei}}{J_i} + \frac{f_i}{J_i} \omega_{mi}$. During the sliding mode and in permanent regime, $\dot{S}_{\omega i} = 0$, $S_{\omega i} = 0$ and $i_{sqi_n}^{ref} = 0$, the equivalent control can be given as (6).

$$i_{sqi_{eq}}^{ref} = \frac{1}{\mu_i \varphi_{rdi}} \left(\dot{\omega}_{mi}^{ref} + \frac{T_{ei}}{J_i} + \frac{f_i}{J_i} \omega_{mi} \right) \quad (6)$$

During the convergence mode, the condition $\dot{S}_{\omega i} S_{\omega i} < 0$ should be verified and the discontinue control can be expressed as (7).

$$i_{sqi_n}^{ref} = K_{\omega i} \text{Sgn}(S_{\omega i}) \quad (7)$$

Finally, the quadratic current reference is given by (8).

$$i_{sqi}^{ref} = K_{\omega i} \text{Sgn}(S_{\omega i}) + \frac{1}{\mu_i \varphi_{rdi}} \left(\dot{\omega}_{mi}^{ref} + \frac{T_{ei}}{J_i} + \frac{f_i}{J_i} \omega_{mi} \right) \quad (8)$$

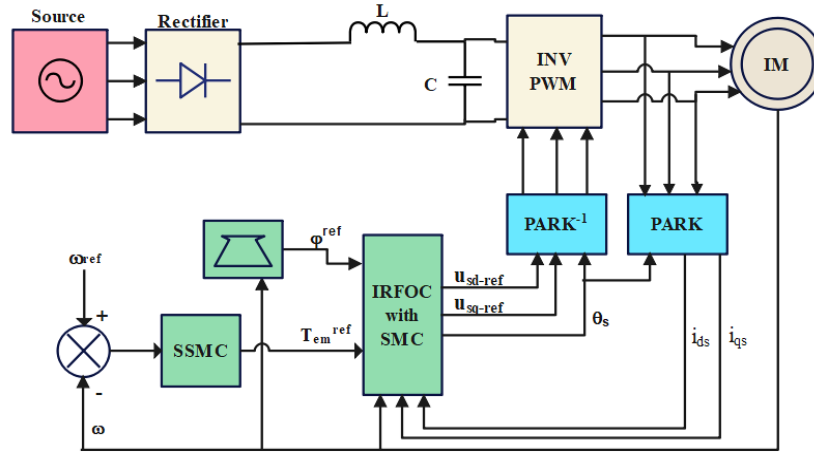


Figure 5. Cascaded sliding mode control of induction motor

3.2.2. Rotor flux controller

The flux surface is chosen as follows: $S_{\phi i} = \phi_i^{ref} - \phi_i$ and the derivative of the surface is given by: $\dot{S}_{\phi i} = \dot{\phi}_i^{ref} - \dot{\phi}_i$. During the sliding mode and in permanent regime, $\dot{S}_{\phi i} = 0$, $S_{\phi i} = 0$ and $i_{sdi_n}^{ref} = 0$, the equivalent control can be given as (9).

$$i_{sdi_{eq}}^{ref} = \frac{1}{a_i R_{ri} L_{mi}} (\dot{\phi}_i^{ref} + a_i R_{ri} \varphi_{rdi}) \quad (9)$$

During the convergence mode, the condition $\dot{S}_{\phi i} S_{\phi i} < 0$ should be verified and the discontinue control can be expressed as (10).

$$i_{sdi_n}^{ref} = K_{\phi i} \text{Sgn}(S_{\phi i}) \quad (10)$$

Finally, the direct current reference is given by (11).

$$i_{sdi}^{ref} = K_{\phi i} \text{Sgn}(S_{\phi i}) + \frac{1}{a_i R_{ri} L_{mi}} (\dot{\phi}_i^{ref} + a_i R_{ri} \varphi_{rdi}) \quad (11)$$

For the indirect rotor field-oriented control (IRFOC) tuning parameters we need two surfaces $S_{i_{sdi}} = i_{sdi}^{ref} - i_{sdi}$ and $S_{i_{sqi}} = i_{sqi}^{ref} - i_{sqi}$ the first for the i_{sdi} regulator and the second for i_{sqi} regulator. Deriving of the two surfaces and considering the equations of the system (2), we find in (12).

$$\begin{cases} \dot{S}_{i_{sdi}} = \frac{di_{sdi}^{ref}}{dt} - \psi_{1i} - \frac{1}{\sigma_i L_{si}} u_{sdi} \\ \dot{S}_{i_{sqi}} = \frac{di_{sqi}^{ref}}{dt} - \psi_{2i} - \frac{1}{\sigma_i L_{si}} u_{sqi} \end{cases} \quad (12)$$

During the sliding mode, $S_{i_{sdi}} = 0, S_{i_{sqi}} = 0, \dot{S}_{i_{sdi}} = 0, \dot{S}_{i_{sqi}} = 0, u_{sdi_n}^{ref} = 0, \text{ and } u_{sqi_n}^{ref} = 0$ and the equivalent control actions are done as (13).

$$\begin{cases} u_{sdi_eq}^{ref} = \sigma_i L_{si} \frac{di_{sdi}^{ref}}{dt} - \sigma_i L_{si} \psi_{1i} \\ u_{sqi_eq}^{ref} = \sigma_i L_{si} \frac{di_{sqi}^{ref}}{dt} - \sigma_i L_{si} \psi_{2i} \end{cases} \quad (13)$$

During the convergence mode, the conditions $\dot{S}_{i_{sdi}} S_{i_{sdi}} < 0$ and $\dot{S}_{i_{sqi}} S_{i_{sqi}} < 0$ must be verified and the discontinuous control actions are given as (14).

$$\begin{cases} u_{sdi_n}^{ref} = K_{i_{sdi}} \text{Sgn}(S_{i_{sdi}}) \\ u_{sqi_n}^{ref} = K_{i_{sqi}} \text{Sgn}(S_{i_{sqi}}) \end{cases} \quad (14)$$

Finally, the two regulators control laws, are given by (15).

$$\begin{cases} u_{sdi}^{ref} = u_{sdi_n}^{ref} + u_{sdi_eq}^{ref} = K_{i_{sdi}} \text{Sgn}(S_{i_{sdi}}) + \sigma_i L_{si} \frac{di_{sdi}^{ref}}{dt} - \sigma_i L_{si} \psi_{1i} \\ u_{sqi}^{ref} = u_{sqi_n}^{ref} + u_{sqi_eq}^{ref} = K_{i_{sqi}} \text{Sgn}(S_{i_{sqi}}) + \sigma_i L_{si} \frac{di_{sqi}^{ref}}{dt} - \sigma_i L_{si} \psi_{2i} \end{cases} \quad (15)$$

The product of the surface and its derivative must be less than or equal to zero for the system to be stable. To ensure this condition, the parameters K_{ϕ_i} , K_{ω_i} , $K_{i_{sdi}}$ and $K_{i_{sqi}}$ should first be taken positive and then adjusted to the appropriate values which correspond to the highest performances of the system. These parameters have been chosen in order to: ensure quick convergence, impose sliding dynamics and convergence, and limit current to a value that allows for maximum torque [20], [21].

Now check this condition by evaluating $S_{\omega_i} \dot{S}_{\omega_i}$ and select K_{ω_i} as (16).

$$\begin{aligned} S_{\omega_i} \dot{S}_{\omega_i} &= S_{\omega_i} \left(\dot{\omega}_{mi}^{ref} + \frac{T_{ei}}{J_i} + \frac{f_i}{J_i} \omega_{mi} \right) - \mu_i \varphi_{rdi} K_{\omega_i} |S_{\omega_i}| \\ \Rightarrow K_{\omega_i} &> \frac{1}{\mu_i \varphi_{rdi}} \left(\dot{\omega}_{mi}^{ref} + \frac{T_{ei}}{J_i} + \frac{f_i}{J_i} \omega_{mi} \right) \end{aligned} \quad (16)$$

We find the conditions for the existence of the sliding mode for surfaces S_{ϕ_i} , $S_{i_{sdi}}$, and $S_{i_{sqi}}$ using the same method.

$$\begin{cases} K_{\phi_i} > \frac{1}{a_i R_{ri} L_{mi}} (\dot{\phi}_i^{ref} + a_i R_{ri} \varphi_{rdi}) \\ K_{i_{sdi}} > \sigma_i L_{si} \left(\frac{di_{sdi}^{ref}}{dt} - \psi_{1i} \right) \\ K_{i_{sqi}} > \sigma_i L_{si} \left(\frac{di_{sqi}^{ref}}{dt} - \psi_{2i} \right) \end{cases} \quad (17)$$

Settling time: generally $\dot{S}_{\omega_i} = -K_{\omega_i} \text{Sgn}(S_{\omega_i})$, therefore if $S_{\omega_i} > 0 \Rightarrow \dot{S}_{\omega_i} = -K_{\omega_i} \Rightarrow dS_{\omega_i} = -K_{\omega_i} dt \Rightarrow \int_{S_{\omega_i}(0)}^{S_{\omega_i}(t_s)} dS_{\omega_i} = \int_0^{t_s} -K_{\omega_i} dt \Rightarrow S_{\omega_i}(t_s) - S_{\omega_i}(0) = -K_{\omega_i} t_s$, or at this time $t_s: S_{\omega_i}(t_s) = 0$. Following these calculations, we can determine the settling time to determine the sliding gains [22], [23].

$$K_{\omega_i} = \frac{|S_{\omega_i}(0)|}{t_{s_ \omega_i}}; K_{\phi_i} = \frac{|S_{\phi_i}(0)|}{t_{s_ \phi_i}}; K_{i_{sdi}} = \frac{|S_{i_{sdi}}(0)|}{t_{s_ i_{sdi}}}; K_{i_{sqi}} = \frac{|S_{i_{sqi}}(0)|}{t_{s_ i_{sqi}}}$$

3.3. Voltage-sag mitigation strategy

The voltage-sag management method consists of two parts: a change in M2 machine's operation mode depending on logical conditions and a change in the control topology. M1 and M2 machines have only one working mode in a typical system and under standard voltage conditions, namely the « motor mode ». Four modes of operation are considered in this proposal, each of which is dependent on grid voltage, DC bus voltage, and process speed. « Motor mode », « Free mode », « Vdc control », and « Stopping mode » are the four options available Figure 5, where:

- Motor mode: M2 machine SMC controller acts as a speed controller, with an external set-point ω_{2ref} , and the speed of the M1 machine is always controlled by the mechanical tension controller, which generates a set-point
- Free mode: M2 machine SMC controller acts as a speed controller, with speed set-point equal to the motor speed ($\omega_{2ref} = \omega$).
- Vdc control: M2 machine controller's speed set-point is replaced by a voltage set-point, the controller gains are changed to allow DC bus voltage control, and M2 machine changes to generator mode as necessary. The system shifts to "free mode" if a rise in DC bus voltage is observed and the voltage dip persists. The system changes to "Stopped" mode if the system speed is reduced below the minimum speed (ω_{min}) and the grid voltage is not restored. This mode enforces a controlled braking of the system. The objective of the control in this case is to keep the rectifier output voltage constant, regardless of the speed and load over a wide range of variation. Furthermore, from the desired value of the DC voltage, it is possible to express the reference power by:

$$V_{DC} i_{dc} = P^* = P_{ele} = T_{e1} \Omega \quad (18)$$

Neglecting the losses, the torque expression can be written as in (19):

$$T_{e1} = \frac{P^*}{\Omega} \quad (19)$$

According to electromagnetic torque (3), the latter can be controlled by the quadrature stator current component i_{sq} [24], [25].

- Stopping mode: SSMC controller for M2 machine in stopping mode works as a speed controller with a zero-speed set-point ($\omega_{2ref} = 0$)

4. SIMULATION RESULTS

A first evaluation of the relevance of the proposed voltage-dip detection algorithm and management strategy is performed by simulation. The described algorithms and the models of the MMS have been implemented in MATLAB/Simulink/SimPowerSystems in order to perform simulations under different conditions. For voltage-sags detection, three distinct estimators are implemented in the "ADALINE sags detection algorithm" block shown in Figure 6. These are S-Functions written in C language. An S-Function is a Simulink block description language that can be written either in MATLAB language, C, C++, and Ada or Fortran. An S-function allows creating new Simulink blocks by the user. This program is then compiled using the "mex" command.

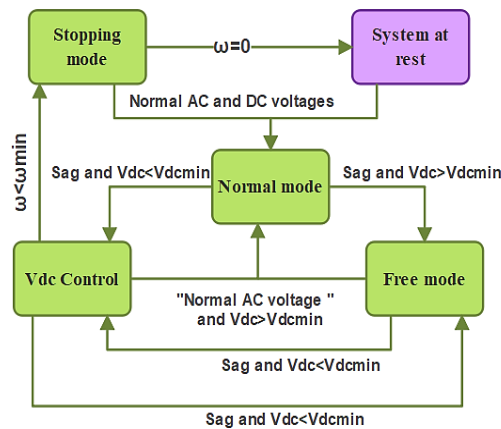


Figure 6. State diagram showing the four operating modes of the voltage-dip management strategy: motor mode, free mode, Vdc control, and stopping mode

“SAG mitigation strategy” block presented in Figure 7, is implemented using Stateflow. This is a state diagram or state-transition scheme consisting of a graphical representation of the finite number of states in a state machine, the state transitions, and the rules that control these. We considered that M1 and M2 machines rotate at different speeds and that they have different moments of inertia. This is the typical case in a material winding system. Mechanical characteristics used in simulation work are listed in Table 1.

Figures 8-15 depict the system's response to a voltage-sag with a depth of 50% and a duration equal to the T_{reg} produced when the system operates at a speed of 70 rad/s. Note that $t = 4s$ represents the start time of the voltage-dip. Furthermore, the difference in speed between roller 1 and roller 2 is negligible. Electromagnetic torques Figure 13 show significant differences, owing to the moments of inertia involved. Trajectories of DC bus voltage as shown in Figure 11, the roller speed is shown in Figure 12 and mechanical tension shown in Figure 14 show that mechanical tension and DC bus voltage can be controlled even if the machines reduce their speed by less than 20%.

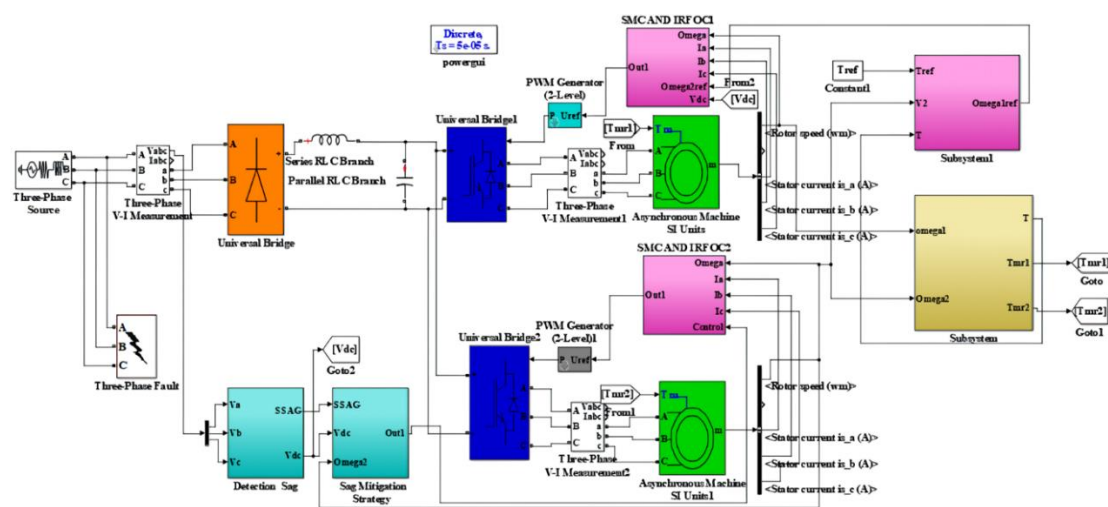


Figure 7. Simulink model of detection algorithm and management strategy

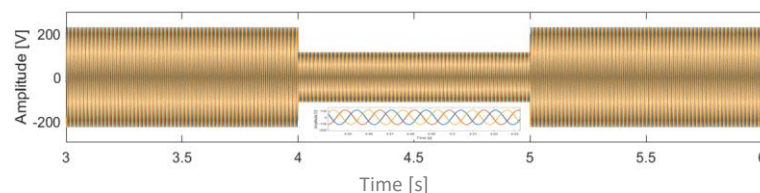


Figure 8. Three-phase fundamental voltages, magnitude signal for symmetrical faults type A

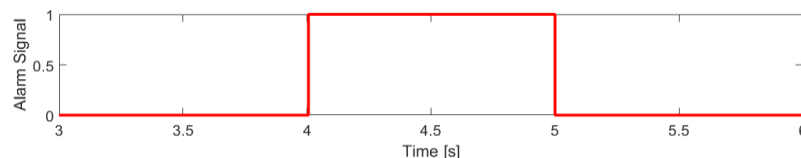


Figure 9. Voltage sag alarm signal

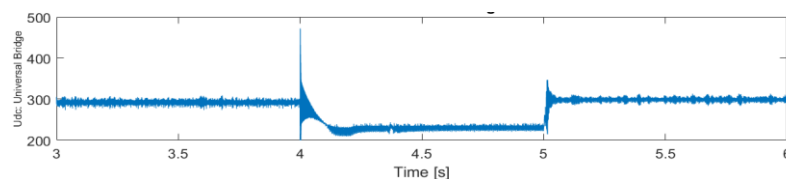


Figure 10. Output voltage waveform from a 3-phase rectifier

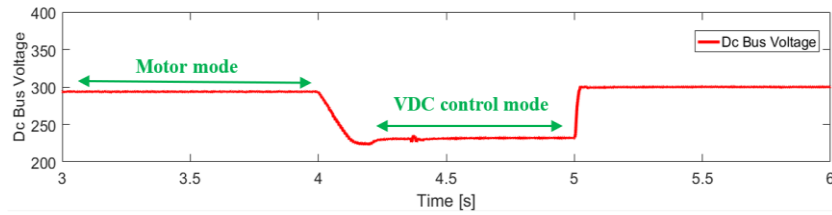


Figure 11. DC-link voltage

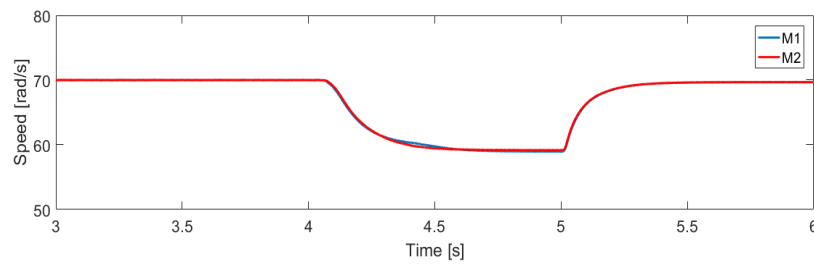


Figure 12. Rollers speed trajectories

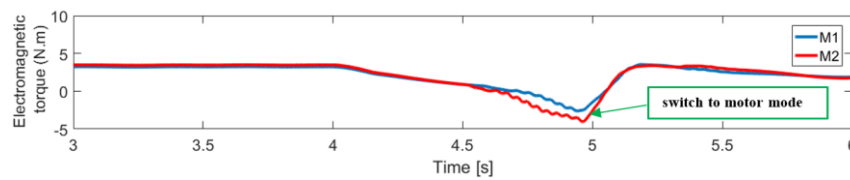


Figure 13. Motors electromagnetic torque

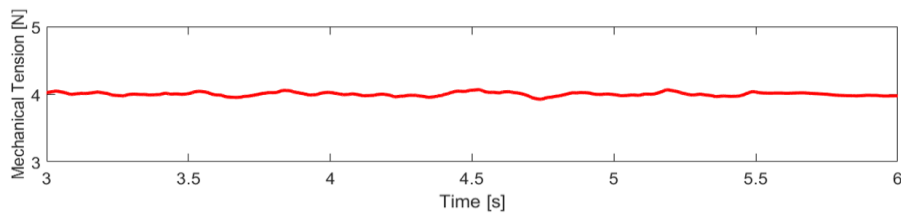


Figure 14. Web mechanical tension

During a voltage-sag, as illustrated in Figure 15, converter 2 supplies current to converter 1 to help M1 machine keep running at the required speed, and to maintain the electrical link current constant. At the end of the voltage-sag, an overcurrent occurred. This is caused by the voltage difference between the DC bus and the voltage supplied by the rectifier. This problem can be avoided by controlling the restart of the rectifier bridge at the end of the voltage-dip.

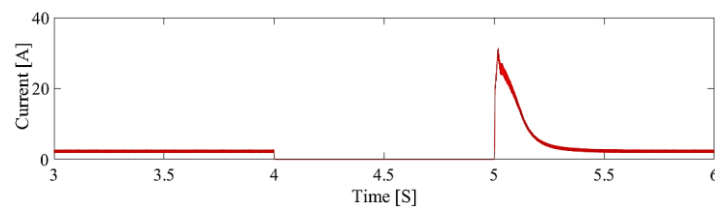


Figure 15. Rectifier output current

5. CONCLUSION

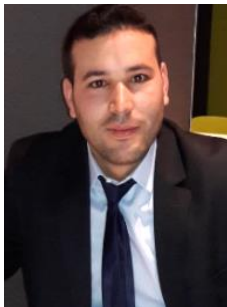
This paper proposed voltage-dip management strategy for a MMS consisting of two asynchronous machines mechanically coupled by an elastic material and connected to a common DC bus. A control system based on the sliding mode was designed, and the stability of the control law was proven. Simulation was used to test the functionality and the relevance of this strategy, and obtained results demonstrated that during the voltage-sag, DC bus voltage was effectively controlled. The significance of rapid detection of the voltage-dip by ADALINE method and the quick correct change of the machine's operation mode has been emphasized. This strategy is based on the measurement of the DC bus voltage to allow its control and to maintain process continuity. Simulation results also showed the efficiency of the proposed strategy to manage the voltage-dip in the coupled MMS, demonstrating that they can operate properly before, during, and after the voltage-dip. However, the system's autonomous operation is limited by the efficiency of the system's total inertia and the operating speed when voltage-dip occurs. The machine's kinetic energy at the start of the voltage dip is a function of the square of the speed at the start of the voltage dip and the inertia. the regulation operating time, determined by the machine's energy at the start of the voltage dip and the power absorbed by the load on the DC bus, corresponds to the case of perfect recovery of the machine's kinetic energy. On the one hand, the goal of future research is to set up an experimental test bench to emulate a mechanically coupled industrial multi-motor system. And secondly, the implementation of a proposed voltage dip management strategy for a mechanically coupled multi-motor system using DSP boards and dSPACE rapid prototyping systems.




REFERENCES

- [1] M. Wang, X. Ren, and Q. Chen, "Robust tracking and distributed synchronization control of a multi-motor servomechanism with H-infinity performance," *ISA Trans.*, vol. 72, pp. 147–160, Jan. 2018, doi: 10.1016/j.isatra.2017.09.018.
- [2] B. Mounir, A. Ba-Razzouk, M. Elharoussi, and B. Rached, "Attenuation of voltage sags effects and dynamic performance improvement of a multi-motor system," *Int. J. Power Electron. Drive Syst.*, vol. 13, no. 2, pp. 705–715, Jun. 2022, doi: 10.11591/ijpeds.v13.i2.pp705-715.
- [3] B. Zhang, S. Mo, H. Zhou, T. Qin, and Y. Zhong, "Finite-Time Consensus Tracking Control for Speed Sensorless Multi-Motor Systems," *Appl. Sci.*, vol. 12, no. 11, p. 5518, May 2022, doi: 10.3390/app12115518.
- [4] A. Bouscayrol *et al.*, "Multi-converter multi-machine systems: application for electromechanical drives," *Eur. Phys. J. Appl. Phys.*, vol. 10, no. 2, pp. 131–147, May 2000, doi: 10.1051/epjap:2000124.
- [5] M. Bensaid, B. Rached, M. Elharoussi, and A. Ba-Razzouk, "Multi-drive electric vehicle system control using backstepping strategy," in *2020 1st International Conference on Innovative Research in Applied Science, Engineering and Technology (IRASET)*, IEEE, Apr. 2020, pp. 1–6. doi: 10.1109/IRASET48871.2020.9092164.
- [6] M. Bensaid, A. Ba-Razzouk, M. Elharoussi, and B. Rached, "Effects of Symmetrical Voltage Sags on Two Induction Motors System Coupled with An Elastic Web," in *2020 IEEE 2nd International Conference on Electronics, Control, Optimization and Computer Science (ICECOCs)*, IEEE, Dec. 2020, pp. 1–6. doi: 10.1109/ICECOCs50124.2020.9314298.
- [7] M. H. Bollen, "Understanding Power Quality Problems: Voltage Sags and Interruptions," in *Wiley-IEEE Press, IEEE Xplore*, 2000, p. 672. [Online]. Available: <https://ieeexplore.ieee.org/book/5270869>
- [8] V. E. Wagner, A. A. Andreashak, and J. P. Staniak, "Power quality and factory automation," *IEEE Trans. Ind. Appl.*, vol. 26, no. 4, pp. 620–626, 1990, doi: 10.1109/28.55984.
- [9] G. Putynkowski, K. Woźny, E. Szycha, and L. Szycha, "Influence of Voltage Sags on the Continuity of the Operation and Lifespan of Single-Phase Industrial Robots," *Coatings*, vol. 11, no. 10, p. 1229, Oct. 2021, doi: 10.3390/coatings11101229.
- [10] J. L. Duran-Gomez, P. N. Enjeti, and B. O. Woo, "Effect of voltage sags on adjustable-speed drives: a critical evaluation and an approach to improve performance," *IEEE Trans. Ind. Appl.*, vol. 35, no. 6, pp. 1440–1449, 1999, doi: 10.1109/28.806060.
- [11] S. C. Shekar, G. R. Kumar, and S. V. N. . Lalitha, "A transient current based micro-grid connected power system protection scheme using wavelet approach," *Int. J. Electr. Comput. Eng.*, vol. 9, no. 1, pp. 14–22, Feb. 2019, doi: 10.11591/ijece.v9i1.pp14-22.
- [12] J. Holtz, W. Lotzkat, and S. Stadtfeld, "Controlled AC drives with ride-through capability at power interruption," *IEEE Trans. Ind. Appl.*, vol. 30, no. 5, pp. 1275–1283, 1994, doi: 10.1109/28.315239.
- [13] D. Knittel, E. Laroche, and H. Koc, "Tension control for winding systems with two degrees of freedom H/sub /spl infin// controller," in *Conference Record of the 2001 IEEE Industry Applications Conference. 36th IAS Annual Meeting (Cat. No.01CH37248)*, Chicago, IL, USA: IEEE, 2001, pp. 576–582. doi: 10.1109/IAS.2001.955478.
- [14] A. Cardenas, P. Sicard, and A. Chérity, "Multi-drive management system to mitigate voltage sags," *Math. Comput. Simul.*, vol. 81, no. 2, pp. 171–179, Oct. 2010, doi: 10.1016/j.matcom.2010.01.006.
- [15] A. Ahmad, M. Lufti Othman, K. K. B. Zainab, H. Hizam, and N. Aziz, "Adaptive ANN based differential protective relay for reliable power transformer protection operation during energisation," *IAES Int. J. Artif. Intell.*, vol. 8, no. 4, pp. 307–316, Dec. 2019, doi: 10.11591/ijai.v8.i4.pp307-316.
- [16] S. Palackappillil and A. E. Daniel, "Switching function parameter variation analysis of a quasi-sliding mode controlled induction motor drive," *Int. J. Power Electron. Drive Syst.*, vol. 13, no. 2, pp. 733–743, Jun. 2022, doi: 10.11591/ijpeds.v13.i2.pp733-743.
- [17] N. V. Quan and M. T. Long, "Sensorless sliding mode control method for a three-phase induction motor," *Electr. Eng.*, vol. 104, no. 5, pp. 3685–3695, Oct. 2022, doi: 10.1007/s00202-022-01578-5.
- [18] Q. Nguyen-Vinh and T. Pham-Tran-Bich, "Sliding mode control of induction motor with fuzzy logic observer," *Electr. Eng.*, vol. 105, no. 5, pp. 2769–2780, May 2023, doi: 10.1007/s00202-023-01842-2.
- [19] M. Habbab, A. Hazzab, and P. Sicard, "Real Time Implementation of Fuzzy Adaptive PI-sliding Mode Controller for Induction Machine Control," *Int. J. Electr. Comput. Eng.*, vol. 8, no. 5, pp. 2883–2893, Oct. 2018, doi: 10.11591/ijece.v8i5.pp2883-2893.
- [20] M. Pudari, S. R. Arya, and R. K. Arya, "An improved Sliding Mode Observer for parameter estimation in induction motor drive with optimised gains," *Aust. J. Electr. Electron. Eng.*, vol. 20, no. 3, pp. 235–250, Jan. 2023, doi: 10.1080/1448837X.2023.2174110.




- [21] M. Touam, M. Chenafa, S. Chekroun, and R. Salim, "Sensorless nonlinear sliding mode control of the induction machine at very low speed using FM-MRAS observer," *Int. J. Power Electron. Drive Syst.*, vol. 12, no. 4, pp. 1987–1988, Dec. 2021, doi: 10.11591/ijpeds.v12.i4.pp1987-1998.
- [22] S. Alvarez-Rodríguez, G. Flores, and N. A. Ochoa, "Variable Gains Sliding Mode Control," *Int. J. Control. Autom. Syst.*, vol. 17, no. 3, pp. 555–564, Feb. 2019, doi: 10.1007/s12555-018-0095-9.
- [23] E. A. Tannuri, A. C. Agostinho, H. M. Morishita, and L. Moratelli Jr, "Dynamic positioning systems: An experimental analysis of sliding mode control," *Control Eng. Pract.*, vol. 18, no. 10, pp. 1121–1132, Oct. 2010, doi: 10.1016/j.conengprac.2010.06.007.
- [24] C. Murali and C. Chengaiah, "Indirect Vector Control for Five-Phase Asynchronous Generator Using Three Level Rectifier in Wind Energy Systems," *Int. J. Electr. Electron. Res.*, vol. 10, no. 4, pp. 1206–1212, Dec. 2022, doi: 10.37391/ijeer.100470.
- [25] J. L. Domínguez-García, O. Gomis-Bellmunt, A. Sudrià-Andreu, and L. Trilla-Romero, "Indirect vector control of an induction generator with LVRT capability," Birmingham, UK: Proceedings of the 2011 14th European Conference on Power Electronics and Applications, 2011, pp. 1–10.

BIOGRAPHIES OF AUTHORS






Mounir Bensaid    was born in Ouazzane, Morocco. He is a Ph.D. student in the "Mathematics, Computer, and Engineering Sciences Laboratory" (MISI), Team: Systems Analysis and Information Processing (ASTI), FST, Hassan First University, Settat, Morocco. He received the Master in Automatic, Signal Processing, and Industrial Computing from the Science and Technical Faculty, Hassan First University, Settat, Morocco, in 2018. His research consists in modeling, characterization, control, and optimization of multi-drive systems. He can be contacted at email: mo.bensaid@uhp.ac.ma.



Abdellfattah Ba-Razzouk    received the Master's degree (M.Sc.A.) in industrial electronics from the Université du Québec à Trois-Rivières (UQTR), Quebec, Canada, in 1993, and the Ph.D. degree in electrical and computer engineering from the École Polytechnique de Montréal, Quebec, Canada, in 1998. From 1997 to 2003, he was a Lecturer in "Motors modeling and control" at the Department of Electrical and Computer Engineering, UQTR. In September 1998, he joined the Hydro-Quebec Industrial Research Chair on Power and Electrical Energy, UQTR, where he has been a professional research scientist working on "High-Performance Intelligent Control of Electrical Drives". Since June 2009, he has been a professor in electrical engineering with the Department of Applied Physics and a researcher affiliated with the "Systems Analysis and Information Processing Laboratory" and head of the "Systems Analysis and Information Processing Team", all at the Science and Technical Faculty, Hassan First University, Settat, Morocco. His research interests include high-performance control of adjustable-speed drives, parameter identification and adaptive control of electrical motors, neural networks, real-time embedded control systems, renewable energy systems, modeling and computer-aided design, and real-time simulation of power electronics systems using multiprocessor platforms. He can be contacted at email: barazzou@yahoo.ca.



Mustapha El Haroussi    was born in Azilal, Morocco, in 1974. He received his Ph.D. in Error Correcting Codes from Mohammed V University, Morocco, in 2013. In 2014, he joined, as Professor, the "Applied Physics Department" of FST, Hassan First University, Settat, Morocco. He can be contacted at email: m.elharoussi@gmail.com.